Engine-in-the-Loop Validation of a Frequency Domain Power Distribution Strategy for Series Hybrid Powertrains

Youngki Kim[1]. Tulga Ersal[1]. Ashwin Salvi[1]. Zoran Filipi[2]. Anna Stefanopoulou[1].

[1]University of Michigan, Ann Arbor, MI 48105 USA
(e-mail:{youngki, tersal, asalvi, annastef}@ umich.edu).

[2]Clemson University, GreenVille, SC 29607 USA
(e-mail: zfilipi@ clemson.edu).

Abstract: This paper presents an engine-in-the-loop validation of a power management strategy for hybrid electric powertrains that splits the power demanded by driver between the engine and battery depending on the frequency content. In particular, a series hybrid electric powertrain is considered where the engine is a real 6.4L diesel engine and the rest of the vehicle, including the battery, generator, motors, vehicle dynamics, and driver, is modeled in computer. A networked engine-in-the-loop experiment is considered where the engine and generator constitute one site, and the rest of the system constitutes another site. This networked setup is used to compare the abovementioned power management strategy to a thermostatic strategy as the baseline. For the specific drive cycle considered, the proposed strategy yields about 12% increase in fuel economy, a performance that exceeds the previously reported purely model-based simulation results. In addition, an improvement in battery life can also be expected.

Keywords: power management, hybrid electric vehicles, hardware-in-the-loop simulation, batteries, validation

1. INTRODUCTION

Vehicle powertrain hybridization is one of the promising technologies for improved fuel economy and reduced tailpipe emissions, where hydraulic accumulators or batteries are used in conjunction with internal combustion engines. Various different topologies for hybridization have been explored; e.g., series (Filipi and Kim, 2010, Jalil et al., 1997), parallel (Liu et al., 2008, Yang et al., 2012, Zheng et al., 2010), and power split (or series-parallel) (Liu and Peng, 2008, Yanhe and Kar, 2011). They all demonstrated improvements in fuel economy and some showed reduction in emissions.

The hybrid powertrain technology has already been successfully deployed on some passenger vehicles (Duoba et al., 2001, Lave and MacLean, 2002). Heavy-duty military vehicles could benefit from this technology, as well, even though they have significantly different performance goals and driving patterns than those of passenger vehicles. Within the military context, requirements such as silent watch, increased mobility, enhanced functionality for on-board power, and improved export-power capabilities make hybrid electric configurations more attractive than hybrid hydraulic architectures. Among various hybrid electric configurations, the series configuration has drawn interest due to greater flexibility in vehicle design when it comes to considerations such as the V-shaped hull design to maximize the survivability of the crew during blast events (Ramasamy et al., 2009). Therefore, with the specific military application in mind, the focus of this paper is on the series hybrid electric architecture.

The performance of a hybrid powertrain in terms of reducing both fuel consumption and emissions critically depends on the power management strategy; i.e., the supervisory control algorithm that determines how the total power demanded by the driver will be shared between the engine and, for example, the battery. Many power management strategies for series hybrid electric vehicles have been proposed to fully exploit hardware potential for minimizing fuel consumption and emissions (Hochgraf et al., 1996, Caratozzolo et al., 2003, Filipi et al., 2004, Konev et al., 2006, Pisu and Rizzoni, 2006, Kim and Filipi, 2007, Sciarretta and Guzzella, 2007, Di Cairano et al., 2011, Jalil et al., 1997, Li and Feng, 2012).

Among these many strategies proposed, Konev et al. and Di Cairano et al. highlight the importance of a smooth engine operation that will minimize the aggressive transient operation of the engine. This is important because of two reasons: (1) a smooth operation allows the engine to operate close to the steady-state conditions where the operation is optimal in terms of fuel efficiency; and (2) reducing transients also reduces emissions. To achieve such a smooth operation, Konev et al. and Di Cairano et al. propose methods to smoothen the power demand that is required from the engine.

In their work, Konev et al. and Di Cairano et al. focus on the benefits of this strategy from the engine perspective only and within the context of passenger vehicles with spark-ignition engines. The impact of this strategy within context of military vehicles with diesel engines is still an open-research question. The impact of this type of strategy on the battery operation and battery health is also unknown.

Thus, this paper is aimed to investigate the effects of a power-smoothing strategy in a series hybrid electric military vehicle with a diesel engine. The effects are addressed from the perspective of both the engine *and* the battery.

Towards this end, a frequency-domain power distribution (FDPD) strategy is considered that has been proposed in (Kim et al., 2012). The FDPD strategy manages power flow by splitting power demand into low and high frequency components through signal processing. Model-based simulations have shown the method to be capable of achieving: 1) reduced battery electric loads, 2) smooth engine transient; and 3) less fuel consumption. This paper first proposes a new design strategy to tune the frequency-based supervisory controller. Control parameters are systematically optimized through the model-based multi-phase optimization process. Then, for the first time, the method is evaluated experimentally using a networked engine-in-the-loop simulation setup and a military vehicle and driving profile. The battery life is assessed explicitly through battery life estimation using a weighted Ah-throughput model (Serrao et al., 2009, Di Filippi et al., 2010). The thermostatic control strategy is also considered as a baseline power management strategy, and the FDPD is compared to the baseline strategy in terms of performance.

The rest of this paper is organized as follows. Section 2 gives an overview of the power management strategies considered in this paper and also proposes a method to tune the FDPD strategy. Section 3 presents the vehicle system considered as a case study. Results are presented and discussed in Section 4, and conclusions are drawn in Section 5.

2. OVERVIEW OF THE POWER MANAGEMENT STRATEGIES

The primary task of a power management strategy is determining the power flow between the vehicle, engine and battery to minimize a cost function such as fuel consumption and emissions. Specifically, a series hybrid configuration can take advantage of the decoupling of the engine from the wheels to operate the engine around the optimal operating conditions. However, the decrease in total system efficiency due to inherent multiple energy conversions, and other constraints such as battery voltage and current limitations make the power management problem a challenging task. Therefore, the design of power management strategy is important to improve fuel economy while reducing engine emissions and to ensure safe battery operations.

2.1 Thermostatic SOC Control

The thermostatic SOC control strategy, one of heuristic control techniques, has been widely employed for series hybrid electric vehicles (Hochgraf et al., 1996, Caratozzolo et al., 2003, Lee et al., 2011, Li and Feng, 2012). This strategy is advantageous because of its ease of implementation, the effectiveness of SOC regulation, and the improvement of fuel economy. The thermostatic SOC control strategy is considered as a baseline strategy in this study.

The principle of the thermostatic strategy can be summarized as follows. As long as current SOC is higher than the target

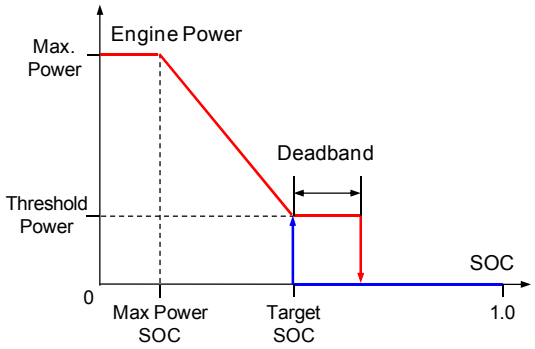

Fig. 1. The schematic of thermostatic SOC control

SOC, the engine provides zero power (Fig. 1). The engine starts charging the battery with the predetermined power level when SOC drops to the target SOC. A dead band is implemented to prevent frequent engine on/off's. When the power demand for vehicle propulsion is higher than the battery discharging power limit, the engine operates in power assisting mode.

However, the thermostatic SOC strategy has several drawbacks. Since the engine is commanded to provide power demand above threshold level, the engine operation changes suddenly and aggressively from zero power demand. This behaviour considerably deteriorates tailpipe emissions (Hagena et al., 2006, Hagena et al., 2011). Moreover, the engine cannot follow the aggressive command because of its large inertia. In terms of improving fuel economy, this strategy cannot avoid multiple power conversions since this strategy prefers using the battery power to the engine/generator power. More importantly, it was found that the Lithium-ion concentration at the surface of solid particles at electrodes can be depleted when high peak currents are drawn from the battery under aggressive conditions, possibly leading to battery degradation through over-discharging (Lee et al., 2011). Based on lessons from previous works, it is necessary to develop a novel power blending strategy with capability of resolving those drawbacks of the thermostatic SOC control strategy.

2.2 Frequency Domain Power Distribution

The separation of power demand in frequency domain provides tailored control inputs to each power source considering different system dynamics. The engine system dynamics is much slower than the battery electrical dynamics. In contrast, the battery can absorb and provide high frequency power demand without delays in responses.

The FDPD is a key enabler to split the total power demand into low frequency and high frequency components. The low frequency components capture the smooth trajectory of the power demand, whereas the high frequency components cover the small amplitude but aggressive and transient power demand. This separation is adequate when system dynamics of the engine and the battery are simultaneously considered. The reduced amplitude of the electric load is beneficial to mitigate electrical stress on the battery. The small amplitude also provides an additional margin for battery downsizing.

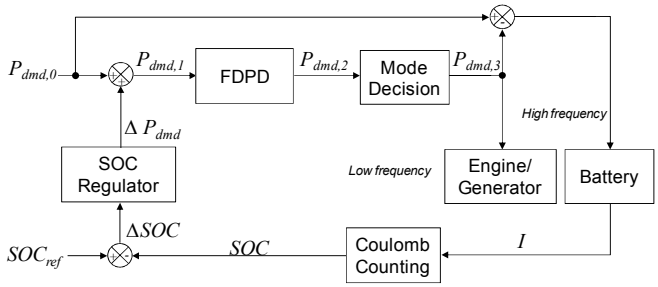

Fig. 2. The schematic diagram of FDPD strategy

Figure 2 shows the structure of the proposed strategy consisting of: 1) FDPD module; 2) SOC regulation module; and 3) mode decision module.

The FDPD module for HEV mode determines the engine/generator power demand by splitting total power demand in low and high frequency ranges. The power demand before deciding a vehicle mode $P_{dmd,2}$ is determined by following steps:

If $P_{dmd,0} \geq P_{th1}$ and $P_{dmd,0} < P_{th2}$

$P_{dmd,1} = P_{dmd,0} + \Delta P_{dmd}$

Else if $P_{dmd,0} \geq P_{th2}$

$P_{dmd,1} = P_{th2} + \Delta P_{dmd}$

Else

$P_{dmd.1} = \Delta P_{dmd}$

$$\tau_{LF} \frac{dP_{dmd,2}}{dt} + P_{dmd,2} = P_{dmd,1}$$

where $P_{dmd,0}$ and $P_{dmd,1}$ are power demand for vehicle propulsion and total power demand respectively. P_{th1} and P_{th2} are threshold power levels for HEV mode incorporated with load-leveling, and τ_{LF} is the time constant of a low-pass filter. The feedback power demand ΔP_{dmd} for the battery SOC regulation is determined through the proportional-integral (PI) controller using the difference between the reference SOC, SOC_{ref} and current SOC

$$\Delta P_{dmd} = k_P \cdot \Delta \mathrm{SOC} + k_I \int \Delta \mathrm{SOC} dt \,, \qquad (1)$$

where k_P and k_I are proportional and integral gain respectively.

The mode decision module determines driving modes. The modes change between an electric-vehicle (EV) mode, a hybrid electric vehicle (HEV) mode and a performance vehicle (PV) mode as following:

If $P_{dmd,2} \leq P_{th1}$

$P_{dmd,3} = 0$: EV mode

Else if $P_{dmd,2} \geq P_{dmd,0} - P_{batt,max}$ & $P_{dmd,2} > P_{th1}$

$P_{dmd,3} = P_{dmd,2}$: HEV mode

Else ($P_{dmd,2} < P_{dmd,0} - P_{batt,max}$) & $P_{dmd,2} > P_{th1}$

$P_{dmd,3} = min(P_{eng,max}, P_{dmd,0} - P_{batt,max})$: PV mode

where $P_{eng,max}$ and $P_{batt,max}$ are maximum available engine power and battery discharging power respectively. Consequently, the performance of FDPD strategy is determined by five control parameters; namely, τ_{LF}, P_{th1}, P_{th2}, k_P, and k_I. These five parameters are determined through a model-based multi-phase optimization process.

2.3 Model-based FDPD Parameter Optimization

In this section, we propose a systematic method to optimize control parameters of the FDPD strategy based on model-based simulation. A hybrid vehicle is a complicated system that includes both energy conversion and energy storage among various power/energy sources. Since numerical round-off, interpolation inaccuracy, and discrete events in the vehicle model simulation lead to discontinuity and computational noise in the objective function (Assanis et al., 1999, Gao and Porandla, 2006), gradient-based optimization algorithms are not frequently used. Thus, multi-phase optimization framework was used in this study to take advantage of both derivative-free (global) and gradient-based (local) optimization algorithms. First, a non-gradient based optimization algorithm aggressively searches for global minimum over a bounded domain. Then, the set is used as an initial point for a gradient-based algorithm with fast convergence. DIRECT is used for the global optimization algorithm because of several advantages (Jones et al., 1993): (1) it searches global and local optimum; (2) tuning parameters is not required; (3) both equality and inequality constraints can be easily handled; (4) it has robust character for nonlinear problems. For local optimization algorithm, Sequential Quadratic Programming (SQP) is used.

The control parameter optimization can be mathematically formulated as following:

Objective : Maximize fuel economy

Constraints :

$$|\Delta v| \leq \Delta v_{ref} \text{ within 1 second}$$
$$SOC_L \leq \mathrm{SOC} \leq SOC_U$$
$$SOC_{end,L} \leq \mathrm{SOC}_{end} \leq SOC_{end,U}$$
$$\mathrm{P}\left(\dot{P}_{\mathrm{eng}} \leq \alpha\right) \geq 95\%$$

Variable Constraints :

$$\tau_{LF} \in \left[\tau_{LF,L}, \tau_{LF,U}\right],\ P_{th1} \in \left[P_{th1,L}, P_{th1,U}\right]$$
$$P_{th2} \in \left[P_{th2,L}, P_{th2,U}\right],\ k_P \in \left[k_{P,L}, k_{P,U}\right]$$
$$k_I \in \left[k_{I,L}, k_{I,U}\right]$$

where Δv the difference between the desired and actual vehicle speeds; the subscripts *ref* and *end* represent the reference and the end of driving cycles; $\dot{P}_{\mathrm{eng}}$ is the derivative of engine power demand with respect to time; and the subscripts L and U denote the lower and upper bounds respectively.

3. DESCRIPTION OF THE CASE STUDY

As a case study, a hybridized Mine Resistant Ambush Protected All-Terrain Vehicle (M-ATV) is considered to explore the effectiveness of the FDPD strategy in severe circumstances, i.e., frequent and high power demand. The specifications of the M-ATV are summarized in Table 1.

Table 1. Vehicle Specification

Component	Specification
Vehicle	Hybridized Mine Resistant Ambush Protected All-Terrain Vehicle (M-ATV)
Weight	14,403 kg
Payload	1814 kg
Frontal Area	5.72 m^2
Engine	6.4L V8 turbo-diesel: 260 kW
Generator	Permanent Magnet: 265 kW
Battery	Li-ion : 9.27 kWh
Motors	Permanent Magnet: 380 kW

A networked engine-in-the-loop simulation (Ersal et al., 2012, Ersal et al., 2011a) of this vehicle system is considered, where the engine is the hardware component and the remaining components of the vehicle system (i.e., generator, battery, motors, vehicle dynamics, and driver) are mathematically modelled. The overview of the networked system architecture is illustrated in Fig. 3.

One of the important considerations in such networked simulation is selecting the location of the coupling point (Ersal et al., 2011b); i.e., how to distribute the models between the two sites. The coupling point significantly affects how much the system dynamics are affected by the network dynamics (e.g., delay). To this end, several options have been considered in this study. All options kept the engine and battery in separate locations in anticipation of a future study with a battery-in-the-loop facility and varied the location of the PMS and Vehicle + Motor models. The configuration shown in Fig. 3 is found to be the best option among the ones considered and has thus been adopted in this study.

The details of the components that comprise the system are given in the rest of this section.

3.1 The Engine-in-the-Loop Setup

The hardware component of interest for this work is a Navistar 6.4L V8 diesel engine with 260 kW rated power at 3000 rpm and a rated torque of 880 Nm at 2000 rpm. It is intended for a variety of medium-duty truck applications covering the range between classes IIB and VII, and features

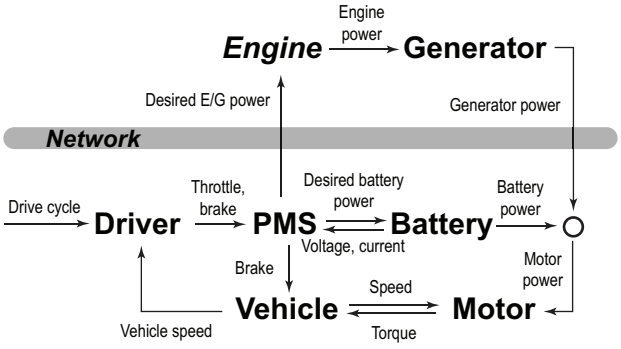

Fig. 3. The overview of the vehicle system simulation architecture used in this case study. Italicized components are physical and the rest remaining ones are simulation models.

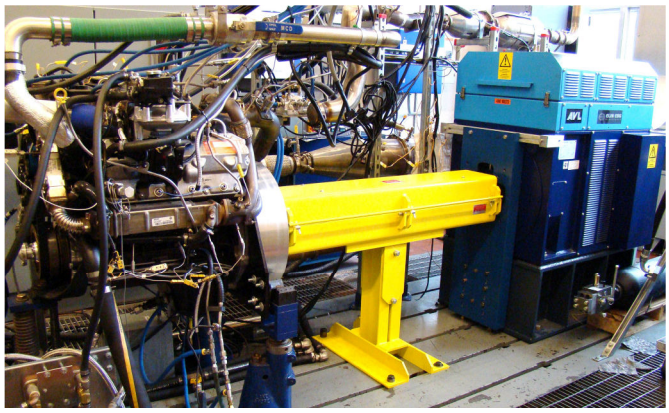

Fig. 4. A photo of the engine-in-the-loop testing facility

technologies such as high pressure common rail fuel injection, twin sequential turbochargers, and exhaust gas recirculation. A high-fidelity, AC electric dynamometer couples the physical engine with the simulation models in real time and operates in speed control mode. The setup can be connected to Simulink for integration with mathematical models, allowing for a real-time hardware-in-the-loop simulation. This connection is achieved through an EMCON 400 flexible test bed with an ISAC 400 extension (Filipi et al., 2006). The photo of the setup is shown in Fig. 4.

3.2 Motor/Generator Model

The motor and the generator are modeled using quasi-steady state efficiency maps under assumption that their dynamics are much faster than vehicle dynamics and transients are negligible. As shown in Fig. 5, the efficiency of the electric machine (EM) η_{EM} is expressed as a function of electrical torque T_{EM} (or electrical Power P_{elec}) and speed ω_{EM} :

$$P_{\text{mech}} = P_{\text{elec}} \cdot \eta_{\text{EM}}^{\ k}, \tag{2}$$

$$\eta_{\text{EM}} = \eta_{\text{EM}}\left(\omega_{EM}, T_{\text{EM}}\right), \tag{3}$$

$$\eta_{EM} = \eta_{EM}\left(\omega_{EM}, P_{elec}\right), \tag{4}$$

where P_{mech} is mechanical power and k indicates the direction of power flow: k=1 represents that electrical power is converted to mechanical power, and k=-1 means that the mechanical power is converted to electrical power. Maximum output torque of the motor T_{max} is governed between the continuous torque curve and the peak torque curve accounting for the heat index α as follows:

$$T_{max} = \alpha\, T_{cont} + (1-\alpha) T_{peak}, \tag{5}$$

$$\alpha = -0.3 - \int \frac{0.3}{\tau_{EM}} \left(\frac{T_{EM}}{T_{cont}} \right) dt, \tag{6}$$

where T_{peak} and T_{cont} are the peak and continuous torque respectively, and these torques are a function of the motor speed (Fig. 7). The heat index varies from zero to one and is used to emulate the change in the torque limit based on motor temperature. The time constant τ_{EM}, of 180 seconds is selected in *Powertrain systems analysis toolkit* developed by Argonne National Laboratory.

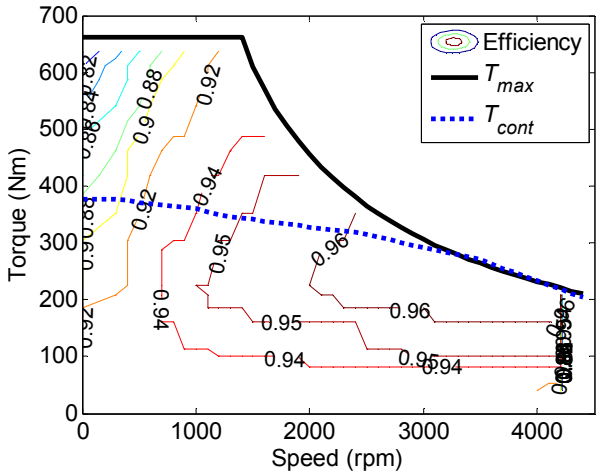

Fig. 5. Efficiency contour map of an electric motor superimposed by maximum and continuous torque

3.3 Optimal Engine/Generator Operation

The best efficient operating points of engine/generator combined system are different from the best engine-efficient operating points. In a series hybrid configuration, the attached generator possibly shifts the best fuel efficient operating points of the combined system to other operating points. The combined system brake specific fuel consumption (*bsfc*) map is obtained by dividing the engine *bsfc* map by the generator efficiency map. The *bsfc* of the engine/generator unit $bsfc_{eng/gen}$ can be calculated by using

$$bsfc_{eng/gen} = bsfc_{eng}/\eta_{gen} \,. \tag{7}$$

The best fuel-efficient operating line is then determined by searching the minimum fuel consumption point for any given power demand. Figure 6 shows the combined $bsfc_{eng/gen}$ and optimal operation line of the engine/generator unit which is used in this study.

3.4 Battery Model

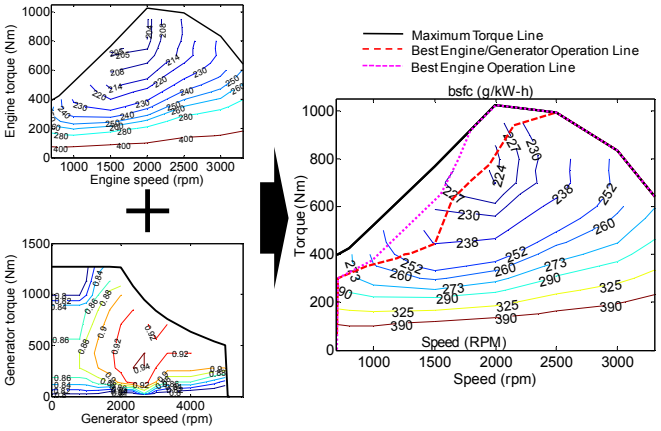

Fig. 6. *bsfc* of engine/generator unit obtained by combining engine *bsfc* and generator efficiency and superimposed by optimal operation lines of the engine/generator unit and the engine only

The battery is modeled using an equivalent circuit approach as shown in Fig. 7. The equivalent circuit model can predict the battery state of charge (SOC) accurate enough to be used in developing a model-based supervisory controller. The open circuit voltage V_{OC} and internal resistances (R_s, R_1, and R_2) and capacitors (C_1 and C_2) during discharging and charging are obtained using parameter identification from the experiments.

Current I and terminal voltage V_t of the battery are calculated by using

$$I = \frac{(V_{OC} - V_{c1} - V_{c2}) - \sqrt{(V_{OC} - V_{c1} - V_{c2})^2 - 4R_s P_b}}{2R_s}, \tag{8}$$

$$V_t = V_{OC} - IR_s - V_{c1} - V_{c2}, \tag{9}$$

where P_b is battery power drawn. V_{c1} and V_{c2} are voltage across the capacitors C_1 and C_2 respectively, and calculated based on the following dynamic equations:

$$\frac{d}{dt}V_{c1} = \frac{1}{C_1}\left(I - \frac{V_{c1}}{R_1}\right), \tag{10}$$

$$\frac{d}{dt}V_{c2} = \frac{1}{C_2}\left(I - \frac{V_{c2}}{R_2}\right). \tag{11}$$

Maximum discharging and charging power limit can be obtained by the following equations:

$$P_{batt,\max} = V_{\min} \cdot I_{\max} = V_{\min}\frac{(V_{OC} - V_{\min})}{R_{\text{int}}}, \tag{12}$$

$$P_{batt,\min} = V_{\max} \cdot I_{\min} = V_{\max}\frac{(V_{\max} - V_{OC})}{R_{\text{int}}}, \tag{13}$$

where I_{min} and I_{max} are the minimum and maximum available current respectively; V_{max} and V_{min} are the manufacturer specified voltage limits. The battery is assumed to be perfectly regulated around a desired temperature so that the effect of temperature is negligible. The battery SOC is predicted based on coulomb counting:

$$\frac{d}{dt}SOC = -\frac{1}{Q}I, \tag{14}$$

where Q is battery capacity. Positive current denotes battery discharging for sign convention.

3.4 Vehicle Dynamics Model

The longitudinal dynamics of the vehicle is calculated by

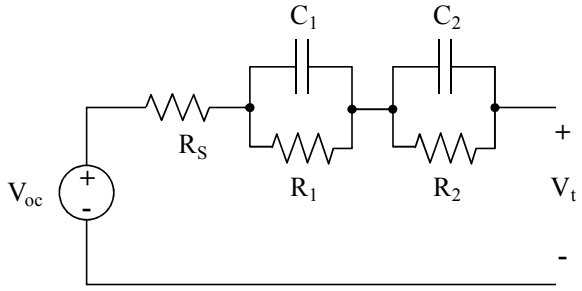

Fig. 7. Equivalent circuit (OCV-R-RC-RC) battery model

using

$$M_{\text{veh}} \frac{dv_{\text{veh}}}{dt} = F_{\text{prop}} - F_{\text{RR}} - F_{\text{WR}} - F_{\text{GR}} - F_{\text{brk}}, \quad (15)$$

where M_{veh} and v_{veh} are the mass and velocity of the vehicle respectively, F_{prop} is the propulsion force, and F_{RR} is the rolling resistance force expressed by

$$F_{\text{RR}} = f_r M_{\text{veh}} g \cos\theta, \quad (16)$$

where f_r is rolling resistance, g is gravitational acceleration, and θ is the road grade. The wind resistance force F_{WR} is calculated by using

$$F_{\text{WR}} = \frac{1}{2} \rho_{\text{air}} C_d A_{\text{veh}} v_{\text{veh}}^2, \quad (17)$$

where ρ_{air} is the air density, C_d is the drag coefficient, and A_{veh} is frontal area of the vehicle. The grade resistance force, $F_{GR} = M_{veh}\ g \sin\theta$, is set to zero in the driving cycles in this study.

3.5 Driver Model

The driver model, which takes the desired and actual vehicle velocities as inputs, is a PI controller with saturation and anti-windup in conjunction with 1, 2, and 3 s preview.

4. EXPERIMENTAL RESULTS AND DISCUSSION

The performance of power management strategies are investigated using an aggressive military driving cycle, *Urban Assault Cycle* (Lee et al., 2011). Frequent high acceleration and deceleration events create aggressive propulsion and braking situations. The velocity profile of this driving cycle is displayed in Fig. 8. The parameters of the baseline thermostatic SOC control and the optimized FDPD strategies are summarized in Tables 2 and 3.

To highlight the performances of the power management strategies, specific time periods are shown in Fig 9. The engine power demand gradually changes under the FDPD strategy. In contrast, the baseline thermostatic SOC strategy always commands engine power demand above threshold

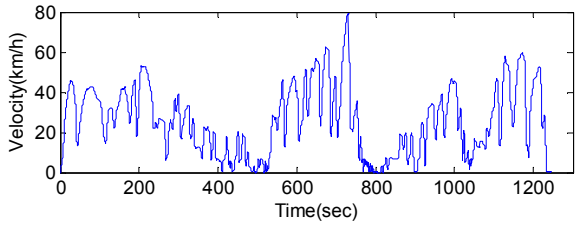

Fig. 8. The speed profile of *Urban Assault Cycle*

Table 2. Parameters of the thermostatic SOC strategy

Parameter	Value
Target SOC	0.5
Deadband	0.02
Max. Power SOC	0.05
Max. Power	260 kW
Threshold Power	100 kW

Table 3. Optimized variables of the FDPD strategy

Variable	Value
Cut-off frequency, τ_{LF}	0.0792
Threshold Power 1, P_{th1}	15.6 kW
Threshold Power 2, P_{th2}	105.5 kW
Proportional gain, k_P	13867.2
Integral gain, k_I	3302.5

level. Moreover, it can be seen that the diesel engine cannot follow an aggressive step-like command due to the slow dynamics; therefore, the battery has to provide the remaining propulsion power until the engine power demand is satisfied. This difference between command and response during transients can be decreased by the FDPD strategy. Furthermore, the FDPD strategy does not emphasize battery charging as much as the thermostatic SOC control does, since it often sends part of the power output directly to the traction motors. This behavior reduces multiple power conversions, which improves system efficiency. As seen from Fig. 10, the cumulative fuel consumption can be decreased under the FDPD strategy. Specifically, the fuel economy is improved from 3.03 km/l to 3.40 km/l by 12 percent compared to the thermostatic SOC control over the over *Urban Assault Cycle*.

The battery SOC and current per cell are compared in Fig. 11. The duration of high current rate can be considerably decreased during aggressive acceleration and deceleration. Figure 12 shows the histogram of battery cell operation and engine operation with two power management strategies. It can be seen that high current conditions and aggressive

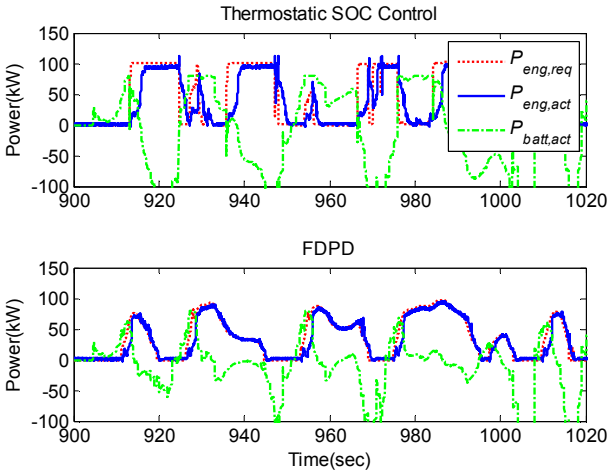

Fig. 9. Comparison of engine power demand, actual engine power, and battery power demand under different power management strategies

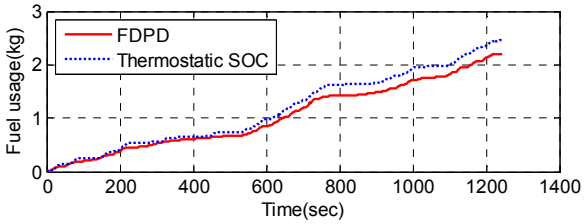

Fig. 10. Comparison of cumulative fuel consumption under different power management strategies

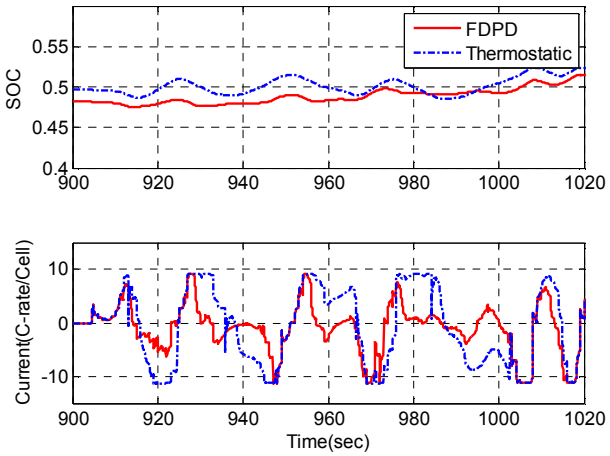

Fig. 11. Comparison of SOC and current per cell under different power management strategies

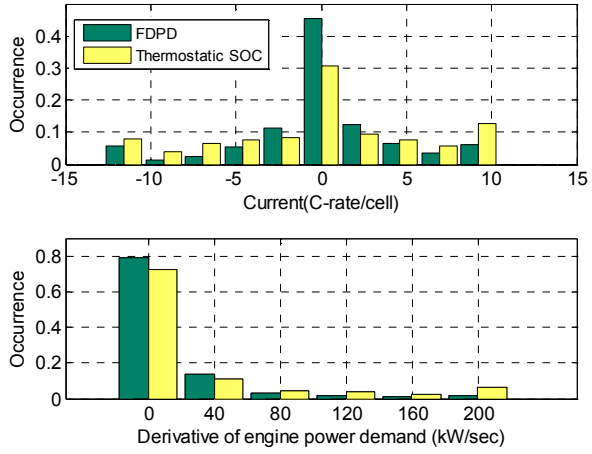

Fig. 12. Histogram of battery cell operation and engine operation

engine power demand (as quantified by the engine power rate) are significantly reduced in case of FDPD strategy, leading to the decrease of average and deviation of current inputs. This behavior is possibly beneficial for the prolonged battery life as well as the reduced emissions. It is noticed that both control strategies show that SOC is regulated around the target value 0.5; however, the FDPD strategy effectively reduces the duration of high current operations.

Battery degradation over the driving cycle is explicitly estimated by using the weighted Ah-throughput model introduced by Serrao and Onori in 2009. This approach uses the linear cumulative damage concept to analyze battery degradation. Since operating conditions such as temperature and current rate affect the degree of degradation, the severity factor w, a nonlinear function, was introduced. The effective accumulated Ah-throughput is calculated by using

$$Ah_{eff} = \int w|I|dt \,. \tag{18}$$

As mentioned in the model description section, operating temperature is assumed to be regulated perfectly. Thus, the severity factor becomes a function of current rate only. Due to the narrow operating range of the battery SOC, the severity factor is assumed to be constant in this paper as a first approximation. The FDPD can considerably decrease the Ah-throughput, resulting in less electrical stress on the battery. Specifically, the FDPD provides a 33% reduction of Ah-throughput over the *Urban Assault Cycle* compared to the thermostatic SOC strategy.

5. CONCLUSIONS

The original contributions of this paper can be summarized as follows. A control parameter tuning strategy has been proposed for the frequency-domain power distribution strategy (FDPD). Control parameters are systematically determined through the model-based multi-phase optimization process, where non-gradient and gradient based algorithms are sequentially combined to take advantage of both algorithms.

A case study has been conducted to experimentally compare the performance of the FDPD to the thermostatic SOC control strategy as the baseline. A networked engine-in-the-loop simulation platform has been developed for this purpose and a Mine Resistant Ambush Protected All-Terrain Vehicle (M-ATV) has been considered as the vehicle system.

The results show that the FDPD strategy successfully reduces aggressive engine power demand and excessive electric battery loads while improving fuel economy by 12% compared to the baseline strategy in the specific scenario considered. The smooth engine power demand results in the decrease of high current rate operation of the battery during propulsion. In addition, battery life is explicitly compared by using the weighted Ah-throughput model. The results show that the FDPD strategy can extend the battery lifespan over typical military driving conditions. The FDPD strategy will be further validated by including a real battery system in the framework.

To the best knowledge of the authors, this paper presents the first effort for investigating the effect of engine power smoothing to the battery operation in a series hybrid electric powertrain. It is also the first to explore the performance of this power management strategy in diesel engines and under military drive cycles.

Future work will compare the FDPD strategy to optimal strategies such as Dynamic Programming and Model-Predictive Control based strategies to investigate the potential of the FDPD strategy further.

REFERENCES

Assanis, D., Delagrammatikas, G., Fellini, R., Filipi, Z., Liedtke, J., Michelena, N., Papalambros, P., Reyes, D., Rosenbaum, D., Sales, A. & Sasena, M. (1999). Optimization Approach to Hybrid Electric Propulsion System Design∗. Mechanics of Structures and Machines, 27 (4), 393-421.

Caratozzolo, P., Serra, M. & Riera, J. (2003). Energy management strategies for hybrid electric vehicles. International Electric Machines & Drives Conference, 241-8.

Di Cairano, S., Liang, W., Kolmanovsky, I. V., Kuang, M. L. & Phillips, A. M. (2011). Engine Power Smoothing Energy

Management Strategy for a Series Hybrid Electric Vehicle. American Control Conference, 2101-6.

Di Filippi, A., Stockar, S., Onori, S., Canova, M. & Guezennec, Y. (2010). Model-based life estimation of Li-ion batteries in PHEVs using large scale vehicle simulations: An introductory study. IEEE Vehicle Power and Propulsion Conference.

Duoba, M., Ng, H. & Larsen, R. (2001). Characterization and Comparison of Two Hybrid Electric Vehicles (HEVs) - Honda Insight and Toyota Prius. SAE 2001 World Congress, Detroit, MI.

Ersal, T., Brudnak, M., Salvi, A., Stein, J. L., Filipi, Z. & Fathy, H. K. (2011a). Development and model-based transparency analysis of an Internet-distributed hardware-in-the-loop simulation platform. Mechatronics, 21 (1), 22-29.

Ersal, T., Brudnak, M., Stein, J. L. & Fathy, H. K. (2012). Statistical transparency analysis in Internet-distributed hardware-in-the-loop simulation. IEEE/ASME Transactions on Mechatronics, 17 (2), 228-238

Ersal, T., Gillespie, R. B., Brudnak, M., Stein, J. L. & Fathy, H. K. (2011b). Effect of Coupling Point Selection on Distortion in Internet-distributed Hardware-in-the-Loop Simulation. American Control Conference.

Filipi, Z. & Kim, Y. J. (2010). Hydraulic hybrid propulsion for heavy vehicles: Combining the simulation and engine-in-the-loop techniques to maximize the fuel economy and emission benefits. Oil and Gas Science and Technology, 65 (1), 155-178.

Filipi, Z., Louca, L., Daran, B., Lin, C. C., Yildir, U., Wu, B., Kokkolaras, M., Assanis, D., Peng, H., Papalambros, P., Stein, J., Szkubiel, D. & Chapp, R. (2004). Combined optimisation of design and power management of the hydraulic hybrid propulsion system for the 6X6 medium truck. International Journal of Heavy Vehicle Systems, 11 (3-4), 372-402.

Filipi, Z. S., Fathy, H. K., Hagena, J., Knafl, A., Ahlawat, R., Liu, J., Jung, D., Assanis, D. N., Peng, H. & Stein, J. L. (2006). Engine-in-the-loop testing for evaluating hybrid propulsion concepts and transient emissions – HMMWV case study. 2006 SAE World Congress, Detroit, MI.

Gao, W. & Porandla, S. K. (2006). Design optimization of a parallel hybrid electric powertrain. IEEE Vehicle Power and Propulsion Conference, 6 pp.

Hagena, J. R., Assanis, D. N. & Filipi, Z. S. (2011). Cycle-resolved measurements of in-cylinder constituents during diesel engine transients and insight into their impact on emissions. Proceedings of the Institution of Mechanical Engineers, Part D: Journal of Automobile Engineering, 225 (9), 1103-1117.

Hagena, J. R., Filipi, Z. S. & Assanis, D. N. (2006). Transient Diesel Emissions: Analysis of Engine Operation During a Tip-In. SAE 2006 World Congress, Detroit, MI.

Hochgraf, C. G., Ryan, M. J. & Wiegman, H. L. (1996). Engine Control Strategy for a Series Hybrid Electric Vehicle Incorporating Load-Leveling and Computer Controlled Energy Management. SAE International Congress & Exposition, Detroit, MI.

Jalil, N., Kheir, N. A. & Salman, M. (1997). A rule-based energy management strategy for a series hybrid vehicle. American Control Conference, 689-693 vol.1.

Jones, D. R., Perttunen, C. D. & Stuckman, B. E. (1993). Lipschitzian optimization without the Lipschitz constant. Journal of Optimization Theory and Applications, 79 (1), 157-181.

Kim, Y., Lee, T.-K. & Filipi, Z. (2012). Frequency Domain Power Distribution Strategy for Series Hybrid Electric Vehicles. SAE 2012 World Congress & Exhibition, Detroit, MI.

Kim, Y. J. & Filipi, Z. (2007). Simulation Study of a Series Hydraulic Hybrid Propulsion System for a Light Truck. SAE 2007 Commercial Vehicle Engineering Congress & Exhibition.

Konev, A., Lezhnev, L. & Kolmanovsky, I. (2006). Control Strategy Optimization for a Series Hybrid Vehicle. SAE 2006 World Congress, Detroit, MI.

Lave, L. B. & Maclean, H. L. (2002). An environmental-economic evaluation of hybrid electric vehicles: Toyota's Prius vs. its conventional internal combustion engine Corolla. Transportation Research Part D: Transport and Environment, 7 (2), 155-162.

Lee, T.-K., Kim, Y., Stefanopoulou, A. & Filipi, Z. S. (2011). Hybrid Electric Vehicle Supervisory Control Design Reflecting Estimated Lithium-Ion Battery Electrochemical Dynamics. American Control Conference, 388-95.

Li, D. & Feng, D. (2012). Thermostatic control for series hydraulic hybrid vehicle (SHHV) energy management. International Conference on Energy and Environmental Protection, 2676-2681.

Liu, J., Hagena, J., Peng, H. & Filipi, Z. S. (2008). Engine-in-the-loop study of the stochastic dynamic programming optimal control design for a hybrid electric HMMWV. International Journal of Heavy Vehicle Systems, 15 (2-4), 309-326.

Liu, J. & Peng, H. (2008). Modeling and control of a power-split hybrid vehicle. IEEE Transactions on Control Systems Technology, 16 (6), 1242-1251.

Pisu, P. & Rizzoni, G. (2006). A supervisory control strategy for series hybrid electric vehicles with two energy storage systems. IEEE Vehicle Power and Propulsion Conference, 8 pp.

Ramasamy, A., Hill, A. M., Hepper, A. E., Bull, A. M. J. & Clasper, J. C. (2009). Blast mines: physics, injury mechanisms and vehicle protection. J R Army Med Corps, 155 (4), 258-64.

Sciarretta, A. & Guzzella, L. (2007). Control of Hybrid Electric Vehicles - A Survey of Optimal Energy-Management Strategies. IEEE Control Systems Magazine, 27 (2), 60-70.

Serrao, L., Onori, S., Rizzoni, G. & Guezennec, Y. (2009). A novel model-based algorithm for battery prognosis. IFAC International Symposium on Fault Detection, Supervision and Safety of Technical Systems, 923-928.

Yang, S., Qi, C., Guo, D., Wang, Y. & Wei, Z. (2012). Topology optimization of a parallel hybrid electric vehicle body in white. International Conference on Mechanical Engineering, Materials and Energy, 668-671.

Yanhe, L. & Kar, N. C. (2011). Advanced design approach of power split device of plug-in hybrid electric vehicles using Dynamic Programming. Vehicle Power and Propulsion Conference, 1-6.

Zheng, W., Zhang, Q. & Cui, S. (2010). Research on the Dynamic Performance and Parameter Design of Parallel Hybrid Electric Vehicle. Advanced Materials Research, 108-111, 613-18.